Efficient Embedded Element Pattern Prediction via Machine Learning
A Case Study with Planar Non-Uniform Sub-Arrays

Onat, Nehir Berk; Roldan, Ignacio ; Fioranelli, Francesco ; Yarovoy, Alexander; Aslan, Yanki

DOI
10.23919/EuCAP57121.2023.10133770

Publication date
2023

Document Version
Final published version

Published in
Proceedings of the 2023 17th European Conference on Antennas and Propagation (EuCAP)

Efficient Embedded Element Pattern Prediction via Machine Learning: A Case Study with Planar Non-Uniform Sub-Arrays

Nehir Berk Onat[1], Ignacio Roldan[2], Francesco Fioranelli[3], Alexander Yarovoy[4], Yanki Aslan[5]
Microwave Sensing, Signals and Systems Group, Department of Microelectronics,
Faculty of Electrical Engineering, Mathematics, and Computer Science,
Delft University of Technology, Delft, The Netherlands
{[1]N.B.Onat, [2]I.Roldanmontero, [3]F.Fioranelli, [4]A.Yarovoy, [5]Y.Aslan}@tudelft.nl

***Abstract*—Efficient prediction of embedded element patterns (EEPs) is including the mutual coupling (MC) effects in the optimization of irregular planar arrays is studied for the first time in the literature. An ANN-based methodology is used to predict the pattern of each element in the whole visible space for a flexible planar array topology in milliseconds. The technique is proposed is validated on a 4-element planar non-uniform sub-array structure. Excellent accuracy on the EEP prediction while providing great efficiency in computational time and load in comparison to the full-wave simulations is demonstrated.**

***Index Terms*— artificial neural network (ANN), embedded element pattern (EEP), irregular antenna array, mutual coupling (MC), phased array antenna.**

I. Introduction

Over the past decades, with the advances in integrated circuit technology, phased array antennas have proven their advantages in achieving high gain, low side-lobe-level (SLL), shaped and multiple agile beams [1]. Therefore, they are widely preferred in wireless communication systems, radar, radio astronomy, and remote sensing [2]. Due to current demands from active integrated phased arrays, such as having reasonable hardware/signal processing complexity, low-cost implementation, fast response time, and low calibration efforts [3], unconventional array architectures are becoming more and more popular [4].

In particular, non-uniformly spaced phased array antennas have attracted wide attention because of their superior potential to achieve better radiation pattern performance, statistical system performance and even thermal performance as compared to the regular arrays [5]. There are several studies in the non-uniform array literature focusing on obtaining a low SLL in a desired field of view (FoV), while having either an optimum number of elements [6], or reconfigurable shaped radiation patterns [7], or multiple steerable pencil beams [8].

Although many studies proposed powerful synthesis techniques for non-uniformly spaced arrays, one crucial challenge, the mutual coupling (MC) effect, was often neglected or has not been efficiently implemented in the synthesis process due to its highly complex nature [9]. However, MC causes significant variations in the embedded element patterns (EEPs) and often degrades the performance of the array pattern. In commonly used iterative synthesis algorithms [8], [10], the obtained EEP for a single element differs in each iteration due to element position change, yielding different interactions between the neighboring elements. This currently makes the reliability of the outcome of the proposed layout optimization techniques questionable.

Various techniques have been proposed to include the MC effects in the synthesis of the non-uniformly spaced arrays, such as infinite-to-finite array approach [11], spherical wave expansion [12]–[14], impedance matrix analysis [15] and the virtual active element pattern expansion method [16]. However, most of the mentioned studies are valid for a particular type of an antenna element, computationally expensive, or do not allow sufficient flexibility in array geometries.

Another and a more straightforward methodology is to perform full-wave simulations during the synthesis to obtain EEPs at each design iteration. Although proven to be effective [17], [18], these techniques increase the computation time and load, which prevent the designers from (i) synthesizing large arrays, (ii) testing different what-if scenarios efficiently for different input parameter selections, (iii) having a large amount of optimized array topologies, and (iv) achieving fast adaptive layout modulation when applicable.

Machine learning (ML) techniques have recently drawn attention due to their potential for efficiently solving non-linear complex problems with remarkable time and accuracy. Specifically, artificial neural network (ANNs) were efficiently used in solving electromagnetics (EM) problems due to their ability to approximate the highly non-linear input-output mappings. Therefore, ML techniques have been exploited in some studies for realistic array pattern estimation and synthesis [19], [20], or to predict EEPs to include MC effects in the synthesis. For the latter, in [21] the author presents an efficient model to achieve accurate MC prediction by building a virtual active element model using Gaussian process regression (GPR). Another recent study aims to include the MC effects in nonuniform linear array synthesis by building a surrogate model for the EEPs using a multi-layer perceptron neural network (MLPNN) [22]. Although the mentioned studies illustrated the potential

of ML in linear non-uniformly spaced arrays, to the best of our knowledge, none of the studies in the literature focus on predicting EEPs in the whole visible space (e.g., in theta-phi, θ, ϕ plane) for a flexible planar irregular array topology.

To fill the mentioned gap in the literature, a novel ANN-based methodology is introduced to predict the EEPs on the θ, ϕ plane in the far field for a planar non-uniform array. A 4-element planar non-uniformly spaced sub-array topology with adjustable element positions is used to test the proposed approach. In our original approach, two neural networks have been cascaded. First, a fully-connected neural network is designed and trained to predict low-resolution EEPs, and then the efficient sub-pixel convolutional neural network (ESPCN) [23] is used to upscale the results to the desired high-resolution. The trained model is planned to be integrated into an optimizer to significantly decrease the computational time and load by efficiently providing the EEPs for the desired sub-array configuration during the optimization process.

The rest of the paper is organized as follows. Section II presents the problem formulation and introduces the case study. Section III explains the proposed ANN structures. Section IV presents the simulation settings with the obtained results. The conclusions are given in Section V.

II. Problem Formulation

The far-field equation for an N-element rectangular array can be formulated as:

$$F(\theta,\phi) = \sum_{n=1}^{N} E_n(\theta,\phi) e^{jk(x_n \sin\theta\cos\phi + y_n \sin\theta\sin\phi)} \quad (1)$$

where $E_n(\theta,\phi)$ is the EEP of the n-th element, $k = 2\pi/\lambda$ where λ is the wavelength at the operating frequency, x_n and y_n indicates the elements positions in x and y coordinates, respectively. During an aperiodic array optimization, the EEPs become quite important due to the change in element positions. The ultimate aim of this study is to accurately estimate the EEP for any given element position, $\hat{E}_n(\theta,\phi)$, which is as close as possible to the full-wave simulated one, $E_n(\theta,\phi)$, in any given array layout with certain constraints (on the maximum aperture size, minimum element spacing etc.). This problem can be simply formulated by the minimization of the mean squared error (MSE):

$$\rho = \frac{1}{NM} \sum_{n=1}^{N} \sum_{m=1}^{M} \left(|E_n^m(\theta,\phi)| - |\hat{E}_n^m(\theta,\phi)| \right)^2 \quad (2)$$

where ρ is the MSE of the given problem and M is the total number of samples for each pattern. For this minimization problem, an ANN framework can efficiently be trained to predict the EEP of an element for a given topology. In this way, the predicted patterns can be provided in real-time with high-precision with a fully-trained network for further use.

In order to realize and test the proposed solution in a small scale, a 4-element planar irregular sub-array architecture that is being studied for a future array design, was chosen for the case study as illustrated in Fig. 1. In this figure, D_n for $n = 1, ..., 4$ indicates the array elements. The n-th element can move on the corresponding element circle which has a fixed origin point O_n and a radius, r_n. Furthermore, the element angle, α_n, is defined as the angle between the x-axis and the radius vector, which is the vector from O_n to E_n.

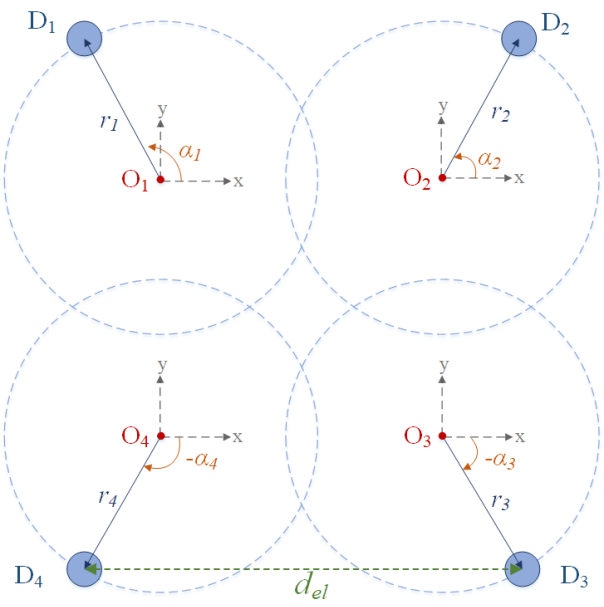

Fig. 1. Irregular sub-array structure for $N = 4$.

In this study, the radius of the the circles are kept equal and the allowable minimum distance between the elements, d_{el}, is defined to be 0.3λ introducing more freedom to the elements and stronger coupling, unlike the conventional 0.5λ minimum element distance constraint. To validate the methodology, dipole antennas are used as an array element where the center frequency was chosen as 12 GHz. The EEPs for the training of the network are generated with CST Microwave Studio and exported in θ, ϕ plane. Since the proposed methodology requires low- and high-resolution data, as explained in the next section, the exported patterns have sizes of 36×36 and 180×180, respectively.

III. Proposed ANN Architecture

Artificial neural networks have been proven to be universal function approximators, given enough layers and sufficient training data [24]. For this reason, an ANN is designed in this work to estimate the EEP of four elements given the array topology. However, it is essential to note that this estimation will be done inside a large aperiodic array optimization algorithm in the future, and thus, the ANN is designed for computational efficiency. Consequently, the size of the networks has been tried to maintain as small as possible.

In this work, the input variables are the four α_n angles, and the goal is to estimate high-resolution EEP (i.e., EEPs discretized every degree) of each element, taking into account

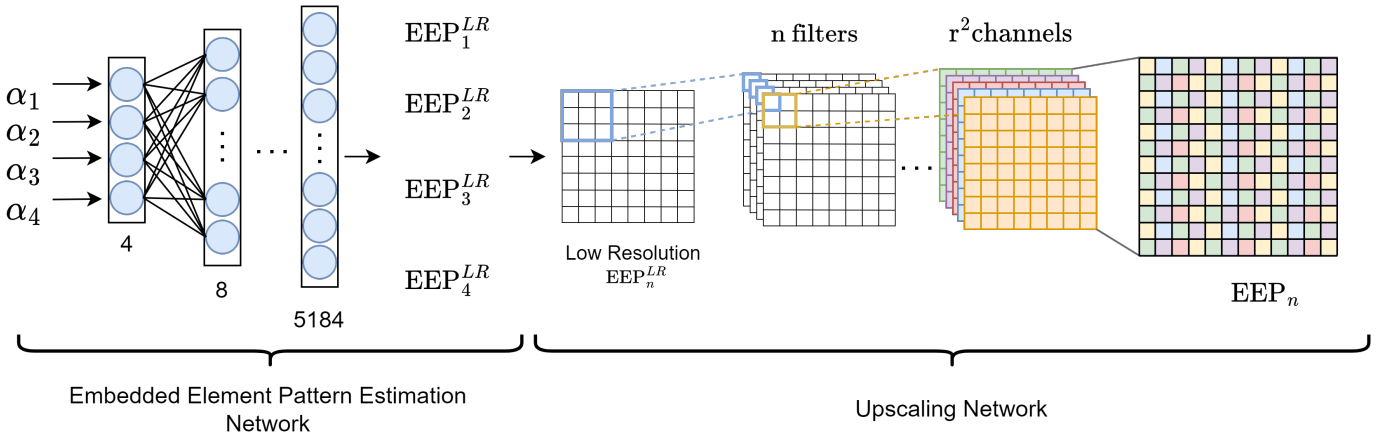

Fig. 2. Block diagram of the proposed neural network architecture. It comprises two networks: the EEP estimation network and the upscaling network. The first one is a fully connected network, while the second is a convolutional neural network based on the ESPCN architecture.

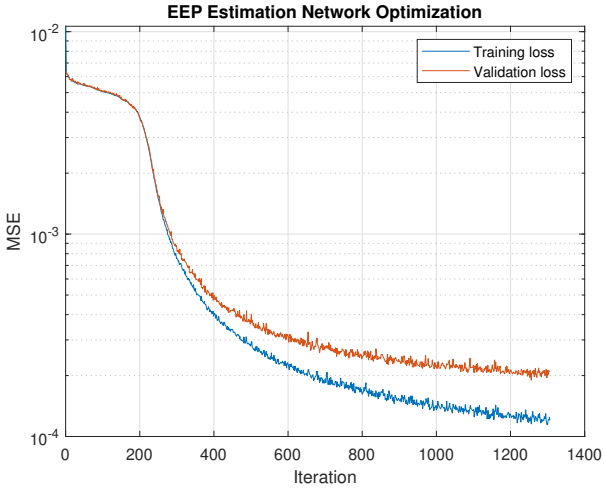

Fig. 3. Evolution of the training and validation loss for the EEP estimation network. The validation loss converges to a value of 2×10^{-4}.

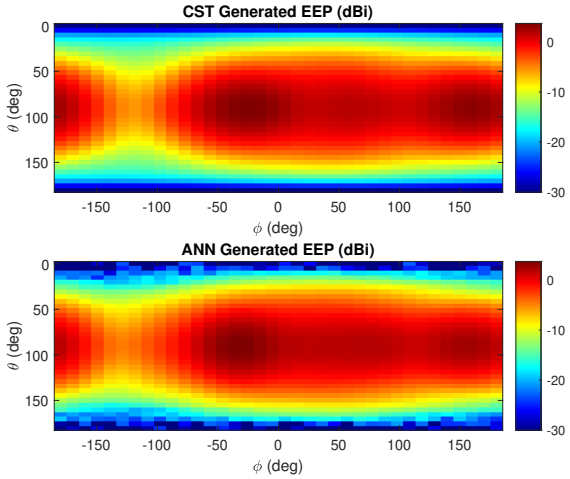

Fig. 4. On the top plot an example of a low-resolution EEP generated with CST. In the lower figure the EEP predicted with the ANN for the same array with the proposed ANN for the same array topology showing very good agreement.

the MC effects. Thus, the number of variables to be estimated is $180 \times 180 \times 4 = 129600$. For this reason, a Feed-Forward NN architecture is unfeasible since it will require an enormous number of parameters to optimize. To overcome this problem, a novel approach that involves the concatenation of two NN is designed, where first low-resolution EEPs are estimated, and then they are upscaled to the desired resolution.

IV. Results

The first ANN is a fully connected network that has as input the four α_n and outputs a low-resolution estimation of the absolute value of each EEP, with 36×36 size. An incremental approach is followed, where the number of layers in each layer is doubled until it reaches 5184 ($36 \times 36 \times 4$), corresponding to the dimension of the four EEP. Therefore, the first ANN consists of 12 layers, the first 11 with a hyperbolic tangent activation function and the last with a linear activation function. Then, once the first network is trained and can acurrately estimate low-resolution EEPs, a second network is designed to upscale them to a higher resolution. With an efficient implementation in mind, the ESPCN network is used, which provides good upscaling performance while maintaining a simple architecture. This network uses two convolutional layers for feature map extraction and a sub-pixel convolution layer that aggregates the feature maps from the low-resolution space and builds the high-resolution image. In this work, the two hidden convolutional layers have n=32 filters and 3×3 kernel size, while the sub-pixel layer has r^2=25 filters to achieve five times the input resolution (upscaling from 36×36 to 180×180). A diagram of these two networks can be seen in Fig. 2.

In total, 9000 random sub-array topology simulations were

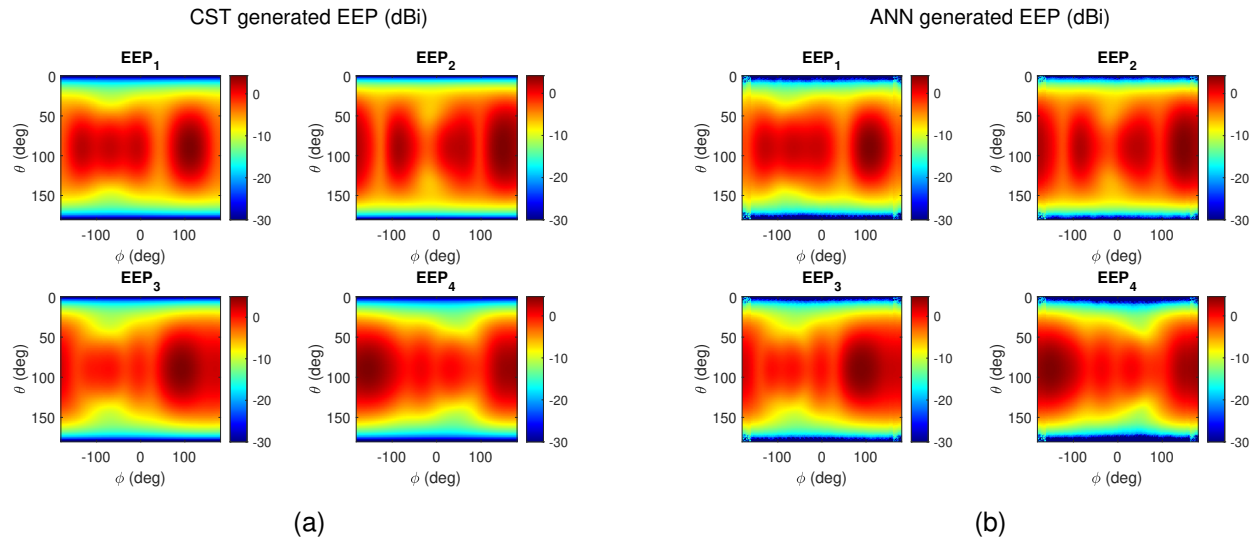

Fig. 5. One example of EEP prediction for a realization where the elements are at 170°, 65°, 175°, and 150°. In (a) the EEPs computed with CST, and in (b) the EEPs computed with the trained neural network.

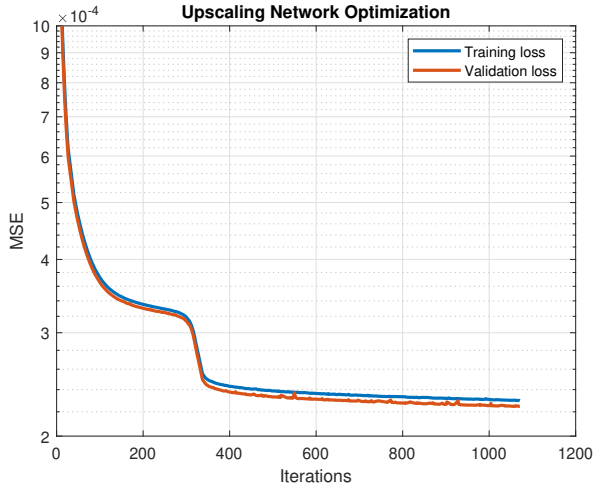

Fig. 6. Evolution of the training and validation loss for the upscaling network. The validation loss converges to a value of 2.1×10^{-4}.

run for the low-resolution dataset by taking into account the minimum element spacing criterion, and 3000 simulations were run for the high-resolution dataset. After each simulation, the EEPs are exported and post-processed with MATLAB to obtain desired input for the proposed ANN models.

As explained in the previous section, the two networks are trained independently, but both use ADAM optimizer [25] with the default hyperparameters (η=0.001, β_1=0.9, β_2=0.999, ϵ=1e-7) and the MSE metric as loss function. The 9000 4-tuple EEPs generated with CST are used as labels using 90% of them for training the networks and 10% for validation. First, the EEP estimation network is trained, and the evolution of the MSE over iterations can be seen in Fig. 3. As expected, the training loss is lower than the validation loss but still converges to a very low value of around 2×10^{-4}. As an example of the output of the trained network, a low-resolution EEP generated with CST and with the network itself is shown in Fig. 4.

Once the first NN is trained, the upscaling network can be concatenated and trained to generate high-resolution EEPs. Fig. 6 shows the evolution of the pixel-wise MSE, and it can be seen how it converges again to a value close to 2.1×10^{-4}. Moreover, now that both networks are trained, the four high-resolution EEPs can be estimated given the four angles. Fig. 5 shows one estimation example for a $\alpha_1 = 170$, $\alpha_2 = 65$, $\alpha_3 = 175$ and $\alpha_4 = 150$, for the CST-generated EEPs and for the ANN-based proposed method. It is important to highlight that the ANN estimation took only 0.15ms, while the computation with CST took 240s.

Finally, it is important to quantify the prediction error, beyond the good visual agreement of Fig. 5a. To this end, the mean error in the peak (ϵ_p) between the CST-generated EEPs and the ANN-generated EEPs is computed over all the validation tests as:

$$\epsilon_\mathrm{p} = 20 \lg \sum_{k=1}^{K} \left(\sqrt{|E_k(\theta_\mathrm{mk}, \phi_\mathrm{mk})|} - \sqrt{|\hat{E}_k(\theta_\mathrm{mk}, \phi_\mathrm{mk})|} \right), \quad (3)$$

with θ_mk and ϕ_mk are the angles where the maximum of the EEP for the k-th element is observed. K is the number of realizations, yielding -39.61dB mean peak error. Moreover, the point-wise error can be computed as:

$$\epsilon(\theta, \phi) = 20 \lg \left(\sqrt{E(\theta, \phi)} - \sqrt{\hat{E}(\theta, \phi)} \right). \quad (4)$$

As an example, the point-wise error for the same antenna configuration is shown in Fig. 7. As can be seen, the error in all the EEPs is very low, with the maximum error for this specific sample being -17.88dB.

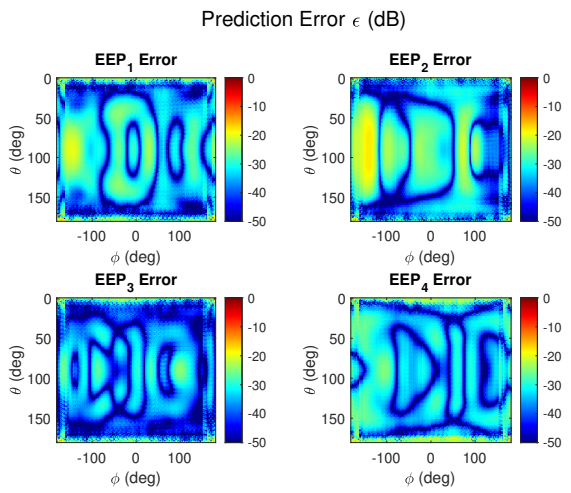

Fig. 7. Point-wise error for the CST and ANN generated EEPs. The elements are at 170°, 65°, 175°, and 150°. The maximum error is -17.88dB

V. Conclusion

An ANN-based methodology has been applied to predict the EEPs of the antenna elements in the whole visible space for a flexible non-uniform array topology. A fully-connected and the ESPCN networks have been concatenated in order to achieve high-resolution in the predicted EEPs. The model has been trained and tested by using a 4-element non-uniform planar sub-array which is currently being used in the development of a large phased array. Excellent agreement between the full-wave simulated and ANN-predicted EEPs has been obtained. The error always remains below -18 dB, which is observed in the low-gain regions, while it is below -30 dB when the gain is relatively high. Future work will focus on extension to the optimization of large irregular phased arrays of patch-type antenna elements where the interaction between the sub-arrays will also be considered.

Acknowledgement

This research was supported by the NWO-NXP Partnership Program on Advanced 5G Solutions and TU Delft Space Institute Seed Grant.

References

[1] J. S. Herd and M. D. Conway, "The evolution to modern phased array architectures," *Proc. IEEE*, vol. 104, no. 3, pp. 519-529, Mar. 2016.

[2] W. Hong et al., "Multibeam antenna technologies for 5G wireless communications," *IEEE Trans. Antennas Propag.*, vol. 65, no. 12, pp. 6231-6249, Dec. 2017.

[3] U. Gustavsson et al., "Implementation challenges and opportunities in beyond-5G and 6G communication," *IEEE J. Microwaves*, vol. 1, no. 1, pp. 86-100, Jan. 2021.

[4] P. Rocca, G. Oliveri, R. J. Mailloux and A. Massa, "Unconventional phased array architectures and design methodologies - a review," *Proc. IEEE*, vol. 104, no. 3, pp. 544-560, Mar. 2016.

[5] Y. Aslan, A. Roederer and A. Yarovoy, "System advantages of using large-scale aperiodic array topologies in future mm-wave 5G/6G base stations: an interdisciplinary look," *IEEE Syst. J.*, vol. 16, no. 1, pp. 1239-1248, Mar. 2022.

[6] G. Oliveri and A. Massa, "Bayesian compressive sampling for pattern synthesis with maximally sparse non-uniform linear arrays," *IEEE Trans. Antennas Propag.*, vol. 59, no. 2, pp. 467-481, Feb. 2011.

[7] O. M. Bucci, T. Isernia and A. F. Morabito, "An effective deterministic procedure for the synthesis of shaped beams by means of uniform-amplitude linear sparse arrays," *IEEE Trans. Antennas Propag.*, vol. 61, no. 1, pp. 169-175, Jan. 2013.

[8] Y. Aslan, J. Puskely, A. Roederer and A. Yarovoy, "Multiple beam synthesis of passively cooled 5G planar arrays using convex optimization," *IEEE Trans. Antennas Propag.*, vol. 68, no. 5, pp. 3557-3566, May 2020.

[9] H. Singh, H. L. Sneha, and R. M. Jha, "Mutual coupling in phased arrays: a review," *Int. J. Antennas Propag.*, vol. 2013, pp. 1–23, Apr. 2013.

[10] B. Fuchs, A. Skrivervik and J. R. Mosig, "Synthesis of uniform amplitude focused beam arrays," *IEEE Antennas Wirel. Propag. Lett.*, vol. 11, pp. 1178-1181, Oct. 2012,

[11] J. I. Echeveste, M. A. Gonzalez de Aza and J. Zapata, "Array pattern synthesis of real antennas using the infinite-array approach and linear programming," *IEEE Trans. Antennas Propag.*, vol. 63, no. 12, pp. 5417–5424, Dec. 2015.

[12] J. Corcoles, J. Rubio and M. A. Gonzalez, "Spherical-wave-based shaped-beam field synthesis for planar arrays including the mutual coupling effects," *IEEE Trans. Antennas Propag.*, vol. 59, no. 8, pp. 2872–2881, Aug. 2011.

[13] J. Corcoles, M. A. Gonzalez and J. Rubio, "Fourier synthesis of linear arrays based on the generalized scattering matrix and spherical modes," *IEEE Trans. Antennas Propag.*, vol. 57, no. 7, pp. 1944-1951, Jul. 2009.

[14] J. I. Echeveste, M. A. Gonzalez de Aza, J. Rubio and C. Craeye, "Gradient-based aperiodic array synthesis of real arrays with uniform amplitude excitation including mutual coupling," *IEEE Trans. Antennas Propag.*, vol. 65, no. 2, pp. 541–551, Feb. 2017.

[15] L. Cen, Z. L. Yu, W. Ser and W. Cen, "Linear aperiodic array synthesis using an improved genetic algorithm," *IEEE Trans. Antennas Propag.*, vol. 60, no. 2, pp. 895-902, Feb. 2012.

[16] Y. Liu, X. Huang, K. D. Xu, Z. Song, S. Yang and Q. H. Liu, "Pattern synthesis of unequally spaced linear arrays including mutual coupling using iterative FFT via virtual active element pattern expansion," *IEEE Trans. Antennas Propag.*, vol. 65, no. 8, pp. 3950-3958, Aug. 2017.

[17] Y. Aslan, M. Candotti, and A. Yarovoy, "Synthesis of multi-beam spacetapered linear arrays with side lobe level minimization in the presence of mutual coupling," *in Proc. 13th EuCAP*, Krakow, Poland, Apr. 2019.

[18] H. B. Van, S. N. Jha, and C. Craeye, "Fast full-wave synthesis of printed antenna arrays including mutual coupling," *IEEE Trans. Antennas Propag.*, vol. 64, no. 12, pp. 5163–5171, Dec. 2016.

[19] C. Cui, W. T. Li, X. T. Ye, P. Rocca, Y. Q. Hei and X. W. Shi, "An effective artificial neural network-based method for linear array beampattern synthesis," *IEEE Trans. Antennas Propag.*, vol. 69, no. 10, pp. 6431-6443, Oct. 2021.

[20] C. Cui, W. T. Li, X. T. Ye, Y. Q. Hei, P. Rocca and X. W. Shi, "Synthesis of mask-constrained pattern-reconfigurable nonuniformly spaced linear arrays using artificial neural networks," *IEEE Trans. Antennas Propag.*, vol. 70, no. 6, pp. 4355-4368, Jun. 2022.

[21] Q. Wu, W. Chen, C. Yu, H. Wang and W. Hong, "Machine learning-assisted array synthesis using active base element modeling," *IEEE Trans. Antennas Propag.*, vol. 70, no. 7, pp. 5054-5065, Jul. 2022.

[22] Y. Gong, S. Xiao and B. -Z. Wang, "An ANN-based synthesis method for nonuniform linear arrays including mutual coupling effects," *IEEE Access*, vol. 8, pp. 144015-144026, Aug. 2020.

[23] W. Shi et al., "Real-time single image and video super-resolution using an efficient sub-pixel convolutional neural network," *in Proc. IEEE Conf. Comput. Vis. Pattern Recognit.*, pp. 1874-1883, Jun. 2016.

[24] K. Hornik, M. Stincheombe and H. White, "Multilayer feedforward networks are universal approximators," *Neural Networks*, vol. 2, pp. 359-366, 1989.

[25] Kingma, D. P., Ba, J. (2014). Adam: A Method for Stochastic Optimization. 1–15.